Radiophysics and Quantum Electronics, Vol. 42, No. 8, 1999

ELF EMISSION GENERATED BY THE HAARP HF-HEATER USING VARYING FREQUENCY AND POLARIZATION

G. M. Milikh,[1] K. Papadopoulos,[1,2]
M. McCarrick,[2] and J. Preston[2]

UDC 537.868

We present first observations of the ELF emission generated by the modulated ionospheric HF-heating using the HAARP facility. We focus primarily on the dependence of the polarization and of the amplitude of the ELF wave upon the frequency and polarization of the heating radio wave. A simple 1D computational model of the ELF generation based on the earlier developed model of a horizontal magnetic dipole caused by the HF ionospheric heating [1] is presented. The model develops a qualitative understanding of the changes in the ELF amplitude and polarization due to variations of the heating frequency. The obtained results imply that polarization of the ELF emission generated by the ionospheric HF-heating can be controlled by changing the frequency or polarization of the radio wave.

1. INTRODUCTION

Generation of VLF/ULF/ELF emission using modulated HF-heating of the lower ionosphere was first reported more than two decades ago [2]. A quasistationary current flowing through the lower ionosphere is disturbed by the HF radiation and in turn irradiates at the modulation frequency. This current is driven by winds in the middle and lower latitude ionosphere, and by the field-aligned mapping of magnetospheric electric fields in the high-latitude ionosphere. A number of experiments have since been conducted using different HF facilities [3–9]. Recently new interest is attracted to the generation of low-frequency emissions due to its possible application to underground explorations [10]. However, in order to conduct underground sensing, both the frequency and polarization of the low-frequency emission have to be controlled. While the frequency of the generated ELF emission is determined by the modulation frequency of the heating radiowave, its polarization is arbitrary. Recent experiments using the HAARP facility which is able to change continuously the frequency and polarization of the emitted radiowave, implied that the polarization could be controlled by a proper choice of the heating frequency.

The objective of this work is to discuss the first observations of the ELF emission generated by the HAARP HF facility, while the primary focus is on the dependence of the polarization and of the amplitude of the ELF wave on the parameters of the heating facility. A simple 1D computational model of the ELF generation by the HF ionospheric heating, based on the earlier results [1], is presented. The model develops a qualitative understanding of the changes in the ELF amplitude and polarization due to variations of the heating frequency.

2. OBSERVATIONS

The ELF emission generated by the modulated HF-heating using the HAARP facility

[1] Department of Physics and Astronomy, University of Maryland, College Park, USA; [2] Advanced Power Technologies, Washington, DC, USA. Translated from Izvestiya Vysshikh Uchebnykh Zavedenii, Radiofizika, Vol. 42, No. 8, pp. 728–735, August 1999. Original article submitted January 11, 1999.

0033-8443/99/4208-0639$22.00

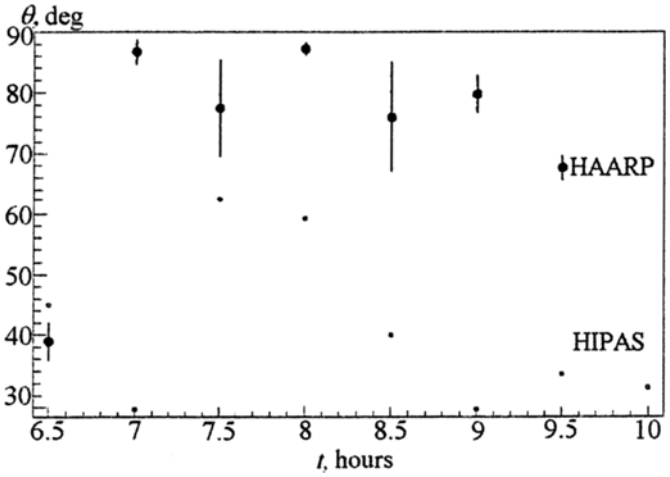

Fig. 1. Polarization angle $\theta = \text{arctg}|B_x/B_y|$ of the ELF emission generated by the HAARP facility (closed circles and bars), and by the HIPAS facility (points).

was observed by the magnetometer at the Gakona site close to the location of the transmitter. The HAARP HF-heater was operating at different frequencies and polarization during 03.12.97 06:30–09:30 UT which corresponds to 23:30–02:30 LT. Either the frequency or polarization was changed each 5 minutes. The continuous HF radiation was modulated by a square wave amplitude with modulation frequency $f_\Omega = 35$ Hz. The amplitudes and phases of the two components of the magnetic perturbations were resolved along the geographically north-south and east-west directions denoted as B_x, B_y and ϕ_x, ϕ_y, respectively. For each of these amplitude or phase components three harmonics (fundamental, third, and fifth) were observed. In order to distinguish effects caused by variations of frequency and polarization of the HF radiation from that due to changing ionospheric conditions, we conducted the HF-heating at the fixed frequency and polarization ($f = 3.155$ MHz, X-mode, $f_\Omega = 28$ Hz) each 30 min during 5-min interval. Simultaneously the ELF emission generated by the HIPAS facility located 290 km south-west of the HAARP site, under similar conditions ($f = 2.85$ MHz, X-mode, $f_\Omega = 28$ Hz), was observed at Gilmore Creek near the HIPAS site and compared with that from the HAARP. Due to the lack of the proper calibration of the ELF emission generated by the HIPAS transmitter, we could not compare the values of the magnetic perturbations B_x and B_y caused by the two above transmitters, but compare instead the corresponding polarization angles $\theta = \text{arctg}|B_x/B_y|$. Note that the value of polarization angle is also affected by the phase difference between B_x and B_y components. This effect will be considered in our future work. The HAARP data were filtered by removing the contaminated data which appear at $1'15''$ at the beginning of each $5'$ interval. We average then the values of θ in $3'45''$ interval and show the mean values and error bars. The HIPAS data were processed by comparing peaks of B_y and B_x within each $5'$ interval.

Figure 1 shows a significant difference between the polarization angle of the ELF emissions generated by the HAARP and HIPAS. We believe that this is due to the different ionospheric conditions at the HAARP and HIPAS sites. Moreover, the polarization angle was almost constant during 07:00–09:00 UT for the HAARP observations. This implies that the ionospheric conditions including the auroral jet direction were constant during this period. This was confirmed by a series of supplementary observations of the ionospheric environment by the time of the heating experiments. In fact, data obtained by the University of Alaska, Geophysical Institute magnetometer located at Gakona show that during the chosen period 03.12.97 07:00–09:00 UT the magnetic variations of all three orthogonal components of the Earth's magnetic field were less then 50γ and did not reveal noticeable time variations. However, both preceding and following periods were characterized by a significant disturbances of the geomagnetic field. In fact, the peak value of the magnetic variations reached was 400γ at about 13:00 UT, which corresponds to a substorm level.

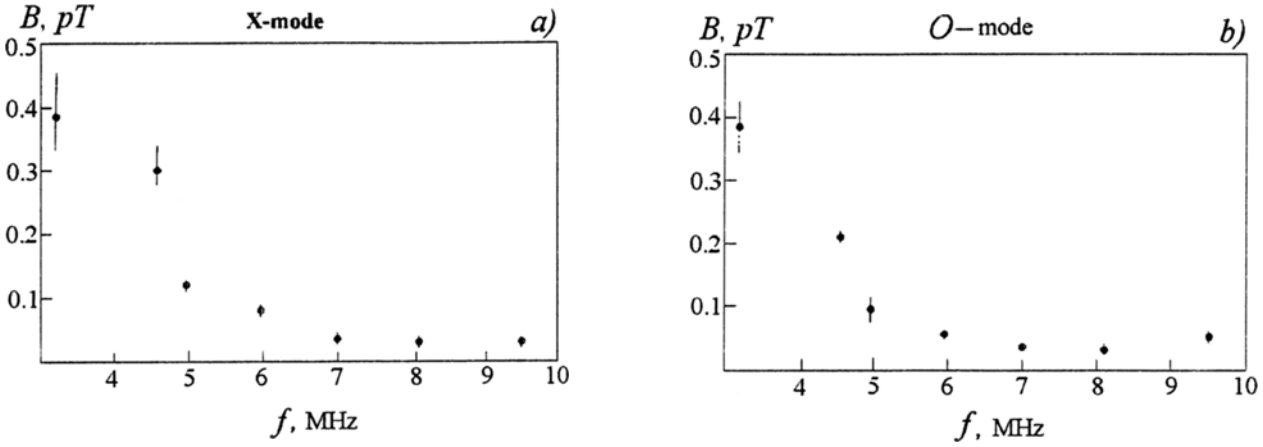

Fig. 2. Amplitude of magnetic perturbations versus the frequency of the heating radio wave of X-mode and O-mode.

Furthermore, the HAARP imaging radiometer showed a moderate ionospheric absorption with no noticeable temporal variations during 03.12.97 07:00–09:00 UT. The UV images taken by the Polar satellite show some auroral activity during 03.12.97 08:45–11:57 UT, unfortunately no observations were made before that time. In short, during the day 03.12.97 some auroral activity took place; however, the time 06:00–09:00 UT presents a quiet period.

In the following analysis we focus on the HAARP data collected during the time 07:00–09:00 UT. During those experiments three different harmonics, namely, the fundamental, third, and fifth, were observed. However, in this paper we discuss the observations of the fundamental harmonic only. Observations of other harmonics will be discussed elsewhere. Figures. 2a and 2b show the amplitude of magnetic perturbation $B = \sqrt{B_x^2 + B_y^2}$ observed at different frequencies of the heating radio wave having X and O-mode. It reveals that B changes with the frequency f as $f^{-\beta}$, $\beta \approx 1 - 2$.

Figures 3a and 3b show the polarization angle of the magnetic perturbation obtained at the same conditions as in Fig. 2a and 2b. The figures reveal a nonmonotonic dependence on the heating frequency.

3. DISCUSSION

As suggested by Zhou et al. [1], the modulated HF-heating excites whistler/helicon waves in the lower ionosphere, which form an expanding loop driven by field-aligned plasma currents. The resulting horizontal magnetic dipole (HMD) radiates the ELF emission of the frequency equal to the modulation frequency f_Ω or its harmonics. Schematics of the ELF emission generated by a horizontal magnetic dipole is shown in Fig. 4. The value of the perturbed magnetic field observed on the ground beneath the HMD, i.e., in the near zone of the ELF emitter, can be obtained if one assumes that it is generated by the two opposite directed currents ΔJ at the bottom and top of the magnetic loop:

$$B = \frac{\mu_0 \Delta J}{2\pi h_c} - \frac{\mu_0 \Delta J}{2\pi (h_c + L)} \simeq \frac{\mu_0 \Delta J}{2\pi h_c} \frac{L}{h_c}, \qquad \Delta J \simeq \mathcal{E} S \cdot \Delta\Sigma. \tag{1}$$

Here $\Delta\Sigma = (\Delta\Sigma_P^2 + \Delta\Sigma_H^2)^1/2$ is the disturbance in the ionospheric conductance caused by the HF-heating, including changes in both Pedersen $\Delta\Sigma_P$ and Hall $\Delta\Sigma_H$ conductances, μ_0 is the magnetic permeability of the vacuum, $\mathcal{E}$ is the ambient electric field, S is the area irradiated by the HF beam, h_c is the height where the ionospheric current induced by the HF-heating is located, and L is the vertical size of the

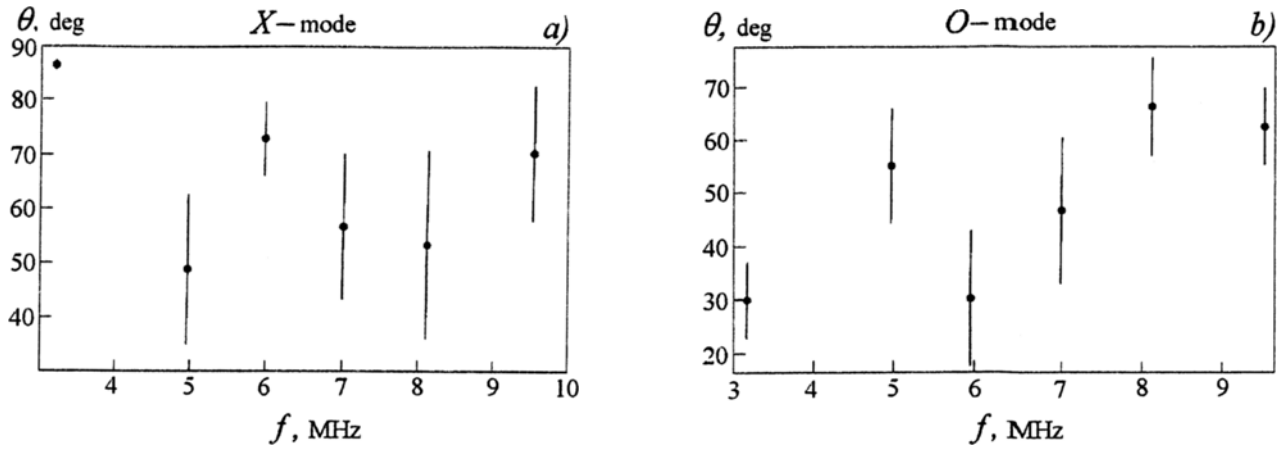

Fig. 3. Polarization angle of magnetic perturbations versus the frequency of the heating radio wave of X-mode and O-mode.

magnetic loop (see Fig. 4). Assuming that the ionospheric current is generated in a thin sheet, the vertical size of the magnetic loop L has the following form [1]:

$$L \simeq (c/\omega_e)\sqrt{\Omega_e t}, \tag{2}$$

where $\omega_e(h_c)$ is the electron plasma frequency at the height h_c, while Ω_e is the local electron gyrofrequency, c is the velocity of light, and t is the loop expansion time.

Furthermore, the polarization angle of the magnetic perturbations induced by the HF-heating is defined by the relation between the magnetic moments of the perturbed Pedersen and Hall currents due to the ionospheric HF-heating. It is illustrated by Fig. 5, where the perturbed Pedersen current ΔJ_P is shown along the polar electrojet making an angle α to the east-west direction, while the perturbed Hall current ΔJ_H is in the orthogonal direction. The magnetic moments due to the Pedersen and Hall perturbed currents M_P and M_H are also depicted in this figure. From this geometry we obtain the B_x and B_y components of the magnetic field disturbances caused by the above magnetic moments, and find then the polarization angle

$$\theta = \operatorname{arctg}|B_x/B_y| = \operatorname{arctg}\left|\frac{(M_P/M_H)\tan\alpha + 1}{M_P/M_H - \tan\alpha}\right|. \tag{3}$$

Using (1) we obtain the ratio of the magnetic moments due to the Hall and Pedersen conductances

$$\frac{M_P}{M_H} = \frac{\Delta J_P L_P}{\Delta J_H L_H} = \frac{\Delta\Sigma_P}{\Delta\Sigma_H}\frac{L_P}{L_H}, \tag{4}$$

where L_H and L_P present the vertical size of magnetic loops due to the Hall and Pedersen current, respectively. We discuss next a numerical model of the ionospheric HF-heating developed in order to calculate the amplitude, as well as the polarization angle of magnetic perturbations induced by the HF heating, and compare them with the observations.

3.1. Computational Model

We consider a simple zero-order 1D model of the ionospheric heating by a series of pulses having square wave modulation. Since the discussed experiments were conducted at a moderate effective radiated power (ERP), we neglect the nonlinear effects including self-absorption in our model. The disturbances in the Hall and Pedersen conductivities due to the HF-heating are given by the following equations:

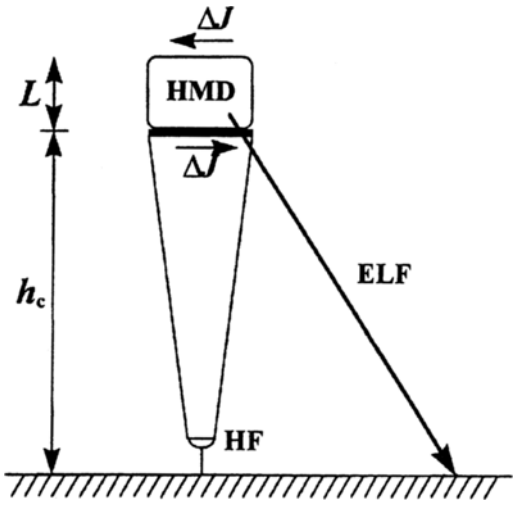

Fig. 4. Schematics of generation of the ELF emission by a horizontal magnetic dipole marked as HMD.

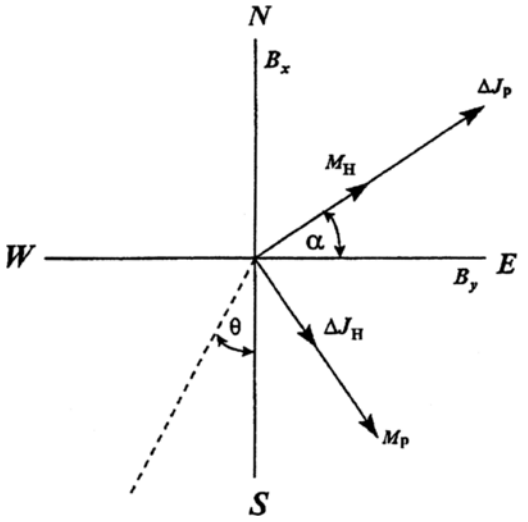

Fig. 5. Relation between the polarization angle θ of the magnetic perturbations and the angle α between the polar electrojet and the west–east direction.

$$\Delta\sigma_H = -\frac{\omega_e^2}{4\pi\Omega_e^2}\frac{2\nu/\Omega_e}{(1+\nu^2/\Omega_e^2)^2}\frac{d\nu}{dT_e}\Delta T_e, \qquad \Delta\sigma_P = \frac{\omega_e^2}{4\pi\Omega_e^2}\frac{1-\nu^2/\Omega_e}{(1+\nu^2/\Omega_e^2)^2}\frac{d\nu}{dT_e}\Delta T_e. \tag{5}$$

Here ν is the electron-neutral collision frequency and the electron heating ΔT_e is given by [11]

$$\Delta T_e = \frac{e^2 E_0^2}{3m\delta_0(\omega^2+\nu^2)}, \tag{6}$$

where $\omega = 2\pi f$ and E_0 are the radio wave frequency and amplitude, m and e are the electron mass and charge, respectively, while δ_0 is the mean fraction of the energy lost by the electron in collision with a neutral particle. The radio wave propagation is described by the equation

$$E_0(z) = E_0(z_0)\left(\frac{z_0}{z}\right)\exp\left\{-\frac{1}{c}\int_{z_0}^{z}\frac{\nu\omega_e^2}{(\omega\pm\Omega_e)^2+\nu^2}\,dz\right\}, \tag{7}$$

where z_0 is the lower boundary of the ionosphere, while + and − correspond to the O and X-mode of the heating radiowave respectively.

Furthermore, we take into account that for a linear disturbances of the electron temperature $\frac{d\nu}{dT_e} = \frac{5}{6}\frac{\nu}{T_e}$ [11]. We adopt then the height dependent electron-neutral collision frequency [11] along with the electron density profile which corresponds to the nighttime ionosphere under conditions of high solar activity [3]. From this model we obtain the altitude dependent perturbations of the Hall and Pedersen conductivity. They are shown in Fig. 6 for the heating wave of X-mode, and for two different frequencies. Here the values $\Delta\sigma_P$, $\Delta\sigma_H$ are normalized over the corresponding peak value of the Hall conductivity. Figure 6 shows that the perturbed Hall conductivity peaks at a lower height than Pedersen, and that the both peaks occur at higher altitudes under the higher frequency of the heating wave. Moreover, this effect is far more pronounced for the Pedersen conductivity, since it is determined by the heating of the upper part of the E-layer, above 70 km.

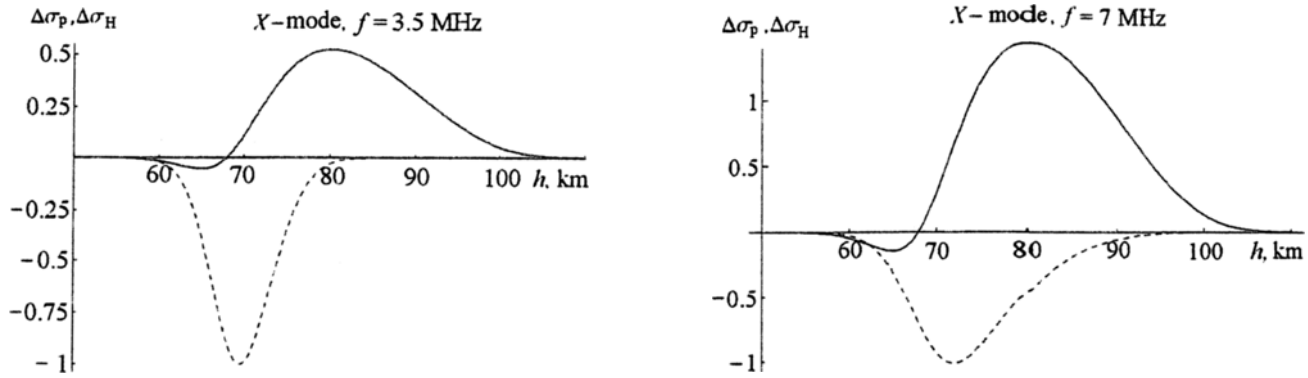

Fig. 6. Disturbances of the Hall (broken trace) and Pedersen (solid trace) conductivities due to the ionospheric heating, normalized over the corresponding peak values of the Hall conductivity for the heating wave of X-mode for the frequencies $f = 3.5$ MHz and $f = 7$ MHz.

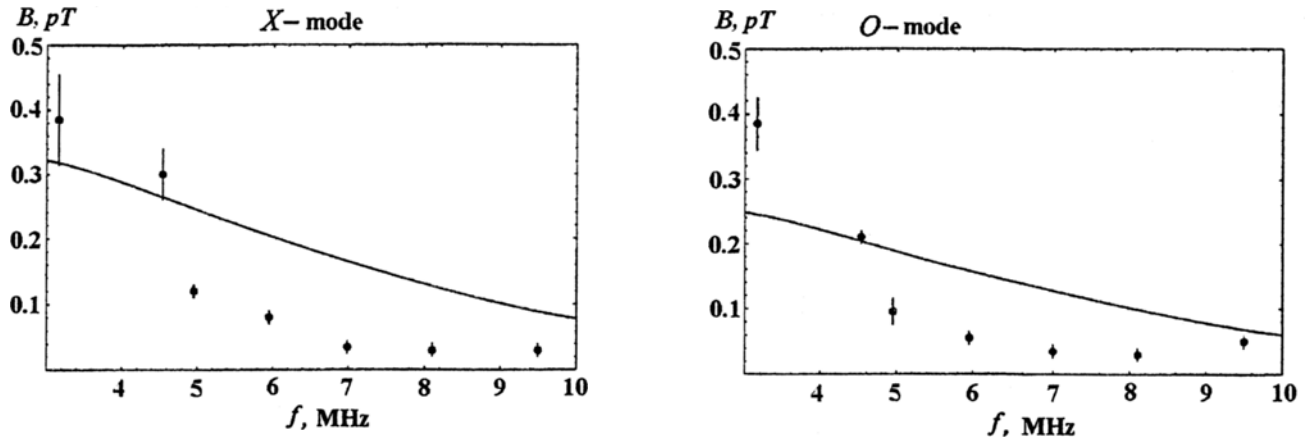

Fig. 7. Amplitude of magnetic perturbations as a function of the frequency of the heating wave along with the relevant observations of the X-mode and of the O-mode.

Assuming next that the ionospheric current is generated mostly in a thin layer whose location coincides with the peak of corresponding conductivity located at the height $h^{\mathrm{H,P}}_{\mathrm{peak}}$, where letters H and P denote the Hall and Pedersen current, we obtain from Eq. (2) that

$$L_{\mathrm{H,P}} \propto 1/\omega_{\mathrm{e}}(h^{\mathrm{H,P}}_{\mathrm{peak}}), \tag{8}$$

where the peak location depends on the heating frequency.

Using Eqs. (1), (5)–(8) we compute the perturbed magnetic field B which could be observed on the ground due to the ionospheric heating by the HAARP transmitter. Figure 7 shows values of B as a function of the frequency of the heating wave along with the corresponding observations for X and O-mode heating wave. Here the effective radiated power (ERP) is considered 10 MW and does not depend on the radiating frequency. In addition, taking into account that the total power of the transmitters is 360 kW, the antenna gain is estimated as 31, so the angle of the main antenna lobe is about 12°. This allows us to evaluate the area S in the ionosphere irradiated by the HF beam. Moreover, the ambient electric field was assumed 3 mV/m, while the size of the HMD magnetic loop is taken as 3 km if the conductivity peaks at 75 km, which corresponds to the heating frequency $f = 3$ MHz.

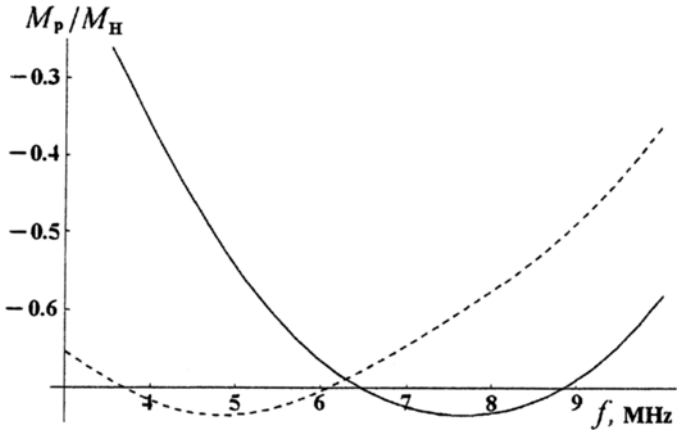

Fig. 8. Ratio of the Pedersen to Hall magnetic moments obtained for the heating wave of X-mode (solid curve), and for the O-mode (broken curve).

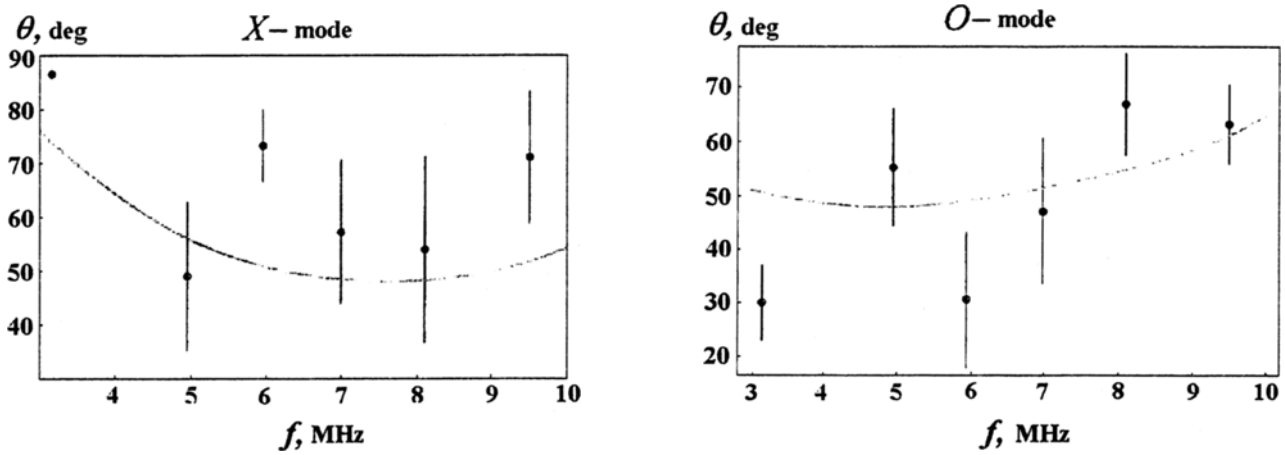

Fig. 9. Polarization angle of magnetic perturbations as a function of the frequency of the heating radio wave of the X-mode, and of the O-mode. Points and bars show observations taken from Fig. 3.

Note that two factors affect the $B(\omega)$ dependence. The first is the variation of the electron temperature which depends on the heating frequency as $\Delta T_e \propto 1/(\omega^2 + \nu^2)$ according to the expression (6). The second is the size of the HMD magnetic loop given by the expression (8). Since the peaks of the Hall and Pedersen conductivities move up when ω increases, raising the plasma frequency $\omega_e(h^{H,P}_{peak})$, both L_H and L_P are reduced with ω.

Furthermore, in order to obtain the polarization angle given by Eq. (3) we compute first the ratio of the Pedersen an Hall conductances Σ_P/Σ_H, and then obtain the ratio of vertical sizes of the corresponding magnetic loops L_P/L_H. The latter depends nonlinearly on the frequency, since the peak of the Pedersen conductivity moves up faster than the peak of the Hall conductivity with increasing ω, as shown by Fig. 6. That allows us to obtain the ratio of Pedersen and Hall magnetic moments from the relation (4), as shown in Fig. 8. Note that the M_P/M_H value experiences a minimum at 4.8 and 7.6 MHz for the X and O-mode correspondingly, due to different dependences of Σ_P/Σ_H and L_P/L_H on ω. We estimate next the value of the angle α between the polar electrojet and east-west direction using the following consideration. First we obtained the ratio of H (north-south) to D (east-west) magnetic field perturbations averaged over 2

hours period of the observations, using the data obtained by the University of Alaska, Geophysical Institute magnetometer located at Gakona. Therefore we found that $B_D/B_H = \tan\theta_{amb} \simeq 0.1$. Furthermore, there is a critical altitude between $70-75$ km where $\nu = \Omega_e$. For altitudes below the critical altitude the dominant current is the Pedersen current, while for the altitudes above the critical altitude the dominant current is the Hall current. Since the electrojet is located mostly above the critical height, the major role is played by the Hall current. Thus neglecting effects caused by the Pedersen current and taking into account that the ambient Hall current is directed similar to the perturbed Pedersen current, we obtain from Fig. 5 that $\tan\alpha = \tan\theta_{amb} \simeq 0.1$.

Finally, by substituting the ratio M_P/M_H along with the value of $\tan\alpha$ into Eq. (3) one can obtain the polarization angle as a function of ω. This is shown in Fig. 9 along with the relevant observations. As follows from Fig. 9, the model is in qualitative agreement with the observations.

4. CONCLUSIONS

First observations of the ELF emission generated by the modulated ionospheric HF-heating using the HAARP facility have been presented. We chose for our analysis the data obtained on 03.12.97 during 07:00–09:00 UT. During this time relatively quiet ionospheric conditions took place, preceded by a significant disturbances of the geomagnetic field.

It was found that the amplitude of magnetic perturbations depends on the heating frequency as $f^{-\beta}$, $\beta \approx 1-2$. The polarization angle ($\theta = \mathrm{arctg}|B_x/B_y|$) reveals a nonmonotonic dependence upon the heating frequency.

A comparison made with a model of the horizontal magnetic dipole generated by the HF heating provides a qualitative explanation of the observed phenomenon.

The obtained results imply that polarization of the ELF emission generated by the ionospheric HF heating can be controlled by changing the frequency or polarization of the heating radio wave.

The authors are indebted to P. N. Guzdar and A. S. Sharma for valuable discussions, and to G. Larionov for helping with the data analysis. The work was supported in part by National Science Foundation under the Grant ATM–9713719.

REFERENCES

1. H. B. Zhou, K. Papadopoulos, A. S. Sharma, and C. L. Chang, *Phys. Plasmas*, **3**, 1484 (1996).
2. G. G. Getmantsev, N. A. Zuikov, T. S. Kotik, L. F. Mironenko, N. A. Mityakov, V. O. Rapoport, Yu. A. Sazonov, V. Yu. Trakhtengerts, and V. Yu. Eidman, *Pis'ma Zh. Éksp. Teor. Fiz.*, **20**, 101 (1974).
3. R. Barr and P. Stubbe, *J. Atmos. Terr. Phys.*, **46**, 315 (1984).
4. R. Barr and P. Stubbe, *J. Geoph. Res.*, **24**, 1403 (1997).
5. R. Barr, P. Stubbe, M. T. Rietveld, and H. Kopka, *J. Geoph. Res.*, **91**, 4451 (1986).
6. P. P. Belyaev, D. S. Kotik, S. N. Mityakov, S. V. Polyakov, V. O. Rappoport, and V. Yu. Trakhtengerts, *Radio Sci.*, **30**, 248 (1987).
7. A. J. Ferraro, H. S. Lee, R. Allshouse, K. Caroll, R. Lunnen, et al., *J. Atmos. Terr. Phys.*, **46**, 855 (1984).
8. D. D. McCarrick, M. J. Sentman, A. Y. Wong, R. F. Wuerker, and B. Chouinard, *Radio Sci.*, **25**, 1291 (1990).
9. H. L. Rowland, M. J. Keskinen, J. S. Villasenor, and A. U. Wong, *J. Geoph. Res.*, **101**, 27027 (1996).
10. D. MacEnany, T. Wallace, R. Shanny, and K. Papadopoulos, "Underground exploration using controlled ionospheric modification," *Nature*, submitted (1998).
11. A. Gurevich, *Nonlinear Phenomena in the Ionosphere*, Springer-Verlag, New York (1978).